Published in final edited form as:

FEBS J. 2014 September ; 281(18): 4123–4137. doi:10.1111/febs.12896.

Structural enzymology and inhibition of the bifunctional folate pathway enzyme HPPK-DHPS from the biowarfare agent *Francisella tularensis*

Gary X. Shaw[1,*], **Yue Li**[2,*], **Genbin Shi**[1], **Yan Wu**[2], **Scott Cherry**[1], **Danielle Needle**[1], **Di Zhang**[1], **Joseph E. Tropea**[1], **David S. Waugh**[1], **Honggao Yan**[2], and **Xinhua Ji**[1]

[1]Macromolecular Crystallography Laboratory, National Cancer Institute, Frederick, MD, USA

[2]Department of Biochemistry and Molecular Biology, Michigan State University, East Lansing, MI, USA

Abstract

Two valid targets for antibiotic development, 6-hydroxymethyl-7,8-dihydropterin pyrophosphokinase (HPPK) and dihydropteroate synthase (DHPS), catalyze consecutive reactions in folate biosynthesis. In *Francisella tularensis* (Ft), these two activities are contained in a single protein, FtHPPK-DHPS. While Pemble and coworkers determined the structure of FtHPPK-DHPS, they were unable to measure the kinetic parameters of the enzyme (*PloS one* **5**, e14165). In this study, we elucidated the binding and inhibitory activities of two HPPK inhibitors (HP-18 and HP-26) against FtHPPK-DHPS, determined the structure of FtHPPK-DHPS in complex with HP-26, and measured the kinetic parameters for the dual enzymatic activities of FtHPPK-DHPS. The biochemical analyses showed that HP-18 and HP-26 have significant isozyme selectivity and that FtHPPK-DHPS is unique in that the catalytic efficiency of its DHPS activity is only $1/2.6\times10^5$ that of *Escherichia coli* DHPS. Sequence and structural analyses suggest that HP-26 is an excellent lead for developing tularemia therapeutics and that the very low DHPS activity is due, at least in part, to the lack of a key residue that interacts with the substrate *p*-aminobenzoic acid (*p*ABA). A BLAST search of 10 *F. tularensis* genomes indicated that the bacterium contains a single FtHPPK-DHPS. The marginal DHPS activity and the singular existence of FtHPPK-DHPS in *F. tularensis* make this bacterium more vulnerable to DHPS inhibitors. Current sulfa drugs are ineffective against tularemia; new inhibitors targeting the unique *p*ABA-binding pocket may be effective and less subject to resistance because mutation may make the marginal DHPS activity unable to support the growth of *F. tularensis*.

Correspondence. Honggao Yan, Michigan State University, 313 Biochemistry Building, East Lansing, MI, 48824, USA; Fax: +1 (517) 353-5282; Tel: +1 (517) 353-9334; yanh@msu.edu, Xinhua Ji, National Cancer Institute, 1050 Boyles Street, Frederick, MD 21702, USA; Fax: +1 (301) 846-6073; Tel: +1 (301) 846-5035; jix@mail.nih.gov.

*These authors contributed equally to this work.

Enzymes

6-hydroxymethyl-7,8-dihydropterin pyrophosphokinase (HPPK, EC 2.7.6.3); dihydropteroate synthase (DHPS, EC 2.5.1.15)

Database

The coordinates and structure factors have been deposited in the Protein Data Bank (PDB) under accession code 4PZV.

Author Contributions

GXS, YL, GS, YW, SC, DN, DZ, and JET performed experiments; DSW, HY, and XJ planned and designed experiments; all authors participated in data analysis; HY and XJ wrote the paper with input from all authors.

Graphical abstract

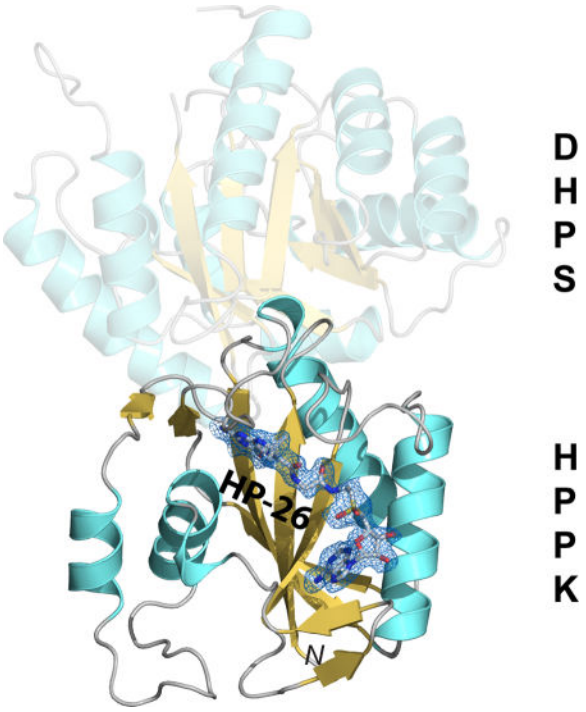

Keywords

HPPK; DHPS; Folate; Antibiotic; *Francisella tularensis*

Introduction

A major target for the development of antimicrobial agents is the folate biosynthesis pathway [1, 2]. Folates are essential for life. Animals obtain folates from their diet, whereas most microorganisms must synthesize folates *de novo* [3]. Among folate pathway enzymes, dihydroneopterin aldolase (DHNA), 6-hydroxymethyl-7,8-dihydropterin pyrophosphokinase (HPPK), dihydropteroate synthase (DHPS), and dihydrofolate synthase (DHFS) are particularly attractive targets of antibiotics because they are absent from mammals. Currently, DPHS inhibitors (sulfonamides) are used in the clinic as antibiotics [4–6], but DHNA, HPPK, and DHFS are not targeted by any existing antibiotics. In most bacteria, these four enzymes exist as monofunctional proteins. However, in some microorganisms, HPPK is fused to the preceding enzyme DHNA forming a bifunctional protein DHNA-HPPK, the following enzyme DHPS forming a bifunctional HPPK-DHPS, or both the preceding and following enzymes forming a trifunctional protein DHNA-HPPK-DHPS [7]. In *Francisella tularensis* (Ft), HPPK is fused to DHPS, forming the bifunctional FtHPPK-DHPS enzyme. Of these four enzymes, the mechanism of HPPK action is best studied and understood [8, 9]. Attempts to inhibit the activity of this enzyme have been made for decades [10–16].

HPPK catalyzes the transfer of pyrophosphate from ATP to 6-hydroxymethyl-7,8-dihydropterin (HP), and produces AMP and 6-hydroxymethyl-7,8-dihydropterin pyrophosphate (HPPP, Fig. 1A) [17, 18]. This pyrophosphoryl transfer reaction follows an apparently ordered kinetic mechanism with Mg^{2+}-dependent ATP binding followed by the rapid addition of HP [19–21]. The catalytically competent active center is assembled when both MgATP and HP are bound [22] and the conformational dynamics of HPPK plays a critical role in both substrate binding and catalysis [9].

DHPS catalyzes the condensation of *p*-aminobenzoic acid (*p*ABA) and HPPP to form dihydropteroate (Fig. 1A), another intermediate in folate biosynthesis. The orally bioavailable sulfonamides function by mimicking *p*ABA and are used in combination with the dihydrofolate reductase inhibitor trimethoprim (co-trimoxazole) against pathogenic organisms, including methicillin resistant *Staphylococcus aureus* (MRSA) [23] and *Pneumocystis carinii* (*jirovecii*) [24]. However, their efficacy has been reduced as a consequence of emerging drug resistance and, therefore, efforts have been made to develop new DHPS inhibitors, including those that bind in the pterin-binding, instead of *p*ABA-binding, pocket of the active site [25].

We have been developing bisubstrate analogue inhibitors of HPPK since 2001 [14] and recently reported two lead compounds: 5'-*S*-[1-(2-{[(2-amino-7,7-dimethyl-4-oxo-3,4,7,8-tetrahydropteridin-6-yl)carbonyl]amino}ethyl)piperidin-4-yl]-5'-thioadenosine (HP-18, Fig. 1B) and 2-amino-7,7-dimethyl-4-oxo-3,4,7,8-tetrahydro-pteridine-6-carboxylic acid (2-{2-[5-(6-amino-purin-9-yl)-3,4-dihydroxy-tetrahydro-furan-2-ylmethanesulfonyl]-ethylcarbamoyl}-ethyl)-amide (HP-26, Fig. 1C) [15, 16]. As shown in Figure 1, the chemical difference between the two inhibitors is the spacer that connects the pterin and the adenosine moieties, an aminoethylpiperidine spacer in HP-18 and a glycyl aminoethyl spacer in HP-26. Although these inhibitors occupy both the pterin- and ATP-binding pockets of HPPK, they exhibit distinct binding modes to *Escherichia coli* HPPK (EcHPPK) and represent two directions for further development [15].

Our strategy for structure-based development of HPPK inhibitors is two-pronged. On one hand, we develop broad-spectrum HPPK inhibitors on the basis of the structure and mechanism of EcHPPK. On the other hand, we fine tune the inhibitor structure in order to develop narrow-spectrum HPPK inhibitors specifically targeting category A biowarfare agents, including *F. tularensis* (tularemia). Structures of FtHPPK-DHPS have been reported in three forms: a ligand-free enzyme, a substrate complex, and an inhibitor complex [26]. However, the enzymatic activity of FtHPPK-DHPS has not been characterized. Here, we report the binding and inhibitory activities of HP-18 and HP-26 against FtHPPK-DHPS, the structure of FtHPPK-DHPS in complex with HP-26, and kinetic parameters for the two enzymatic activities of the protein. We have found that HP-18 is more potent against EcHPPK and HP-26 is more potent against FtHPPK and that FtHPPK-DHPS has a very high K_m for *p*ABA and a very low k_{cat} for the DHPS activity. The results suggest that HP-26 is an excellent lead inhibitor of FtHPPK-DHPS and that inhibition of the bifunctional enzyme is an attractive strategy for the development of tularemia therapeutics.

Results and Discussion

Inhibition of FtHPPK-DHPS by the bisubstrate HPPK inhibitors HP-18 and HP-26

To determine whether HP-18 and HP-26 are also good inhibitors of FtHPPK-DHPS, we measured their IC_{50} values against this enzyme. The results (Table 1) showed that HP-26 is a slightly better inhibitor of FtHPPK-DHPS than EcHPPK, whereas HP-18 is a much poorer inhibitor of FtHPPK-DHPS than EcHPPK. However, IC_{50} values are also dependent on the K_m value of the enzyme and the concentration of the substrate used in the assays. Therefore, we calculated K_i values (Table 1) using the Cheng-Prusoff equation, which takes these two factors into account [27, 28]. The relative magnitudes of the K_i values were consistent with those of the IC_{50} values, indicating that the IC_{50} values are good measurements of the relative potencies of the inhibitors. To further confirm this, we tried to measure the K_d values for these inhibitors by fluorometry. While the K_d value of HP-18 could not be measured because of technical issues such as inner filter effects and solubility, we were able to measure the K_d value of HP-26 for FtHPPK-DHPS binding (Table 1 and Fig. 2). The K_d values of HP-26 also confirmed that the IC_{50} values are good measurements of the potencies of the inhibitors.

HP-26 as an excellent lead for the development of tularemia therapeutics

To understand the structural basis for isozyme selectivity toward the bisubstrate inhibitors, we determined the structure of FtHPPK-DHPS in complex with HP-26 (FtHPPK-DHPS•HP-26, Fig. 3A) at 1.7 Å resolution, but we were unable to co-crystallize FtHPPK-DHPS with HP-18. The electron density of HP-26 is highlighted in Figure 3B; the statistics of X-ray diffraction data and refinement are summarized in Table 2. Previously, three structures of FtHPPK-DHPS, for the isozyme from *F. tularensis* subsq. Holarctica (strain LVS, UniProtKB entry Q2A2W3), were reported: the apo-enzyme, a complex with HP, Mg^{2+}, and the non-hydrolysable ATP analog AMPCPP (FtHPPK-DHPS•HP•MgAMPCPP), and a complex with a DHPS inhibitor (PDB entries 3MCM, 3MCO, and 3MCN) [26]. These structures were not published when we were solving the FtHPPK-DHPS•HP-26 structure. Thus, our structure, for the isozyme from *F. tularensis* subsq. Tularensis (strain SCHU S4, UniProtKB entry Q5NGA7), was determined independently. Including ours, a total of four crystal structures have been determined for this bifunctional enzyme. As expected, the four structures are very similar. For example, the root-mean-square deviation (RMSD) is 0.5 Å for 319 out of 397 pairs of Cα positions between FtHPPK-DHPS•HP•MgAMPCPP (Chain A, PDB entry 3MCO) and FtHPPK-DHPS•HP-26. Among the 78 pairs of Cα positions that were not aligned, 25 are missing from FtHPPK-DHPS•HP•MgAMPCPP and another eight are missing from FtHPPK-DHPS•HP-26. Each of the three previous structures contains two independent FtHPPK-DHPS molecules (Chains A and B) in the asymmetric unit [26], whereas the asymmetric unit of our structure contains only one chain. None of these seven chains is complete and the number of missing residues from each chain ranges from eight to 66. The sequence identity between the two FtHPPK-DHPS proteins is 99.3%. On the basis of FtHPPK-DHPS•HP•MgAMPCPP (PDB entry 3MCO) and FtHPPK-DHPS•HP-26 (this work), a complete model of FtHPPK-DHPS can be derived, which is needed for further development of anti-FtHPPK-DHPS agents.

The RMSD is 0.3 Å for 123 out of 157 pairs of Cα positions between the two HPPK structures in FtHPPK-DHPS•HP-26 and FtHPPK-DHPS•HP•MgAMPCPP (Chain A, PDB entry 3MCO). As shown in Figure 5A, the conformations of these two HPPK backbones are very similar, including the flexible Loop 3 of 11 residues in length. This loop and the arginine residues located at its N- and C-terminus (R82 and R92 in EcHPPK, R87 and R97 in FtHPPK) are strictly conserved among HPPK sequences (Fig. 4). The Loop 3 undergoes unusual conformational changes in the catalytic cycle of HPPK [29, 30]. Concertedly, the two arginine side chains play dynamic roles in the HPPK-catalyzed pyrophosphoryl transfer reaction [31, 32]. The closed conformation of Loop 3 properly positions the R87 and R97 side chains for catalysis. As shown in Figure 5B, R87 interacts with the α-phosphate group while R97 interacts with the β-phosphate group of AMPCPP. Because HPPK-catalyzed reaction involves breaking the ester bond between the α- and β-phosphate groups, this arrangement is consistent with the catalytic stage when the pyrophosphoryl transfer is about to occur [31]. The guanidinium groups of the two arginine side chains in the FtHPPK-DHPS•HP-26 complex are also involved in ligand binding, but in this case both interact with one of the two carbonyl groups in the linker of HP-26 (Fig. 5A, 4B). Interacting with significantly different ligands, the two arginine side chains assume different conformations in the two complexes. Also exhibiting different conformations in the two complexes is the side chain of K79. It interacts with the α-phosphate group of AMPCPP in the substrate complex, but with the 3′ hydroxyl group of the ribose in the inhibitor complex (Fig. 5B). No changes are observed for the interactions between the protein and the ligands' pterin and purine moieties; illustrated in Figure 5C are these interactions observed in FtHPPK-DHPS•HP-26.

As indicated by the enzyme binding and inhibition data (Table 1), HP-26 is a better inhibitor of FtHPPK than EcHPPK. The structures show that both EcHPPK and FtHPPK assume the closed conformation of Loop 3 when they bind HP-26 (Fig. 6A). However, two significant differences can be seen between the two HP-26 complexes. First, the adenine ring system of HP-26 is flipped in the two complexes, which is a dramatic change of the inhibitor conformation. Second, in FtHPPK-DHPS•HP-26, two hydrogen bonds are formed between the conserved R87 and R97 side chains and a linker carbonyl group of the inhibitor, whereas in EcHPPK•HP-26, only one hydrogen bond is formed between the conserved R121 (R126 in FtHPPK-DHPS, Fig. 4) side chain and the linker carbonyl group. Consequently, the conformations of Loop 3 in the two complexes are significantly different (Fig. 6A). It is the interactions between the two catalytic arginine side chains and the inhibitor that dictate the conformation of Loop 3, mimicking that in the ternary complex of the enzyme FtHPPK•HP•MgATP (Fig. 5A). This structural difference can be related to the differing affinity and potency of HP-26 toward the two HPPK enzymes.

The enzyme binding and inhibition data also indicate that HP-18 selectively inhibits EcHPPK (Table 1). Shown in Figure 6B is the structural comparison between the FtHPPK-DHPS•HP-26 and the EcHPPK•HP-18 (PDB entry 3UDE) complexes. In addition to the two conserved arginine side chains, the side chain of an aspartate (D102 in FtHPPK, D97 in EcHPPK) is shown. Also strictly conserved among HPPK sequences, this aspartate side chain coordinates to the two Mg^{2+} ions during catalysis [22]. In FtHPPK-DHPS•HP-26, it occupies two distinct conformations with 0.55 and 0.45 probabilities. In EcHPPK•HP-18

(PDB entry 3UDE), however, it interacts electrostatically with the linker region of the inhibitor. Whether this interaction is possible between FtHPPK-DHPS and HP-18 remains to be seen, but the structural comparison indicates that further modification of the HP-26 linker region such that it also interacts with the D102 side chain (Fig. 6B) may lead to bisubstrate HPPK inhibitors of FtHPPK-DHPS with greatly improved potency.

Kinetic properties of the bifunctional enzyme FtHPPK-DHPS

As the amino acid sequence identities of FtHPPK-DHPS to HPPKs and DHPSs of other organisms are rather low (Fig. 4, 6), it is of great interest to us to determine the kinetic parameters of the enzyme. The results of the kinetic measurements are shown in Figure 8 and summarized in Table 3. Whereas the kinetic parameters for the HPPK activity of the enzyme are similar to those of EcHPPK [21], the kinetic parameters for the DHPS activity of the enzyme are very different from those of *E. coli* DHPS (EcDHPS) [33]. For both FtHPPK-DHPS and EcHPPK, the K_m values for MgATP or HP are in the low μM range and the k_{cat} values less than 1 s^{-1}. In contrast, for the DHPS activity of FtHPPK-DHPS, the K_m value for *p*ABA is 400 times that of EcDHPS and the k_{cat} value is only 0.15% that of EcDHPS. Hence, the catalytic efficiency (k_{cat}/K_m) of FtDHPS is only $1/2.6\times10^5$ that of EcDHPS. Of all the reported DHPSs that have been studied, some of which are listed in Table 3, the FtHPPK-DHPS has the highest K_m for *p*ABA, the lowest k_{cat}, and consequently the lowest catalytic efficiency.

The kinetic behavior of FtHPPK-DHPS is consistent with its amino acid sequence and structure. For the HPPK activity, all of the catalytically important residues are conserved in FtHPPK-DHPS (Fig. 4). Also, the two HPPKs share the same fold (Fig. 6). Not surprisingly, the HPPK activity of FtHPPK-DHPS is very similar to that of EcHPPK. For the DHPS activity, however, a non-conserved active site residue may play an important role. Of the nine DHPSs from diverse microorganisms in Figure 6, six of them, EcDHPS [33], *B. anthracis* DHPS (BaDHPS) [34], *M. tuberculosis* DHPS 1 (MtDHPS1) [35], *S. aureus* DHPS (SaDHPS) [36], *S. cerevisiae* DHPS (ScDHPS, part of a trifunctional enzyme) [37], and *S. pneumoniae* DHPS (SpDHPS) [38], are highly active, whereas FtDHPS is very sluggish (this work) and *M. tuberculosis* DHPS 2 (MtDHPS2) is inactive [39]. While no kinetic parameters have been reported for *Y. pestis* DHPS (YpDHPS), the enzyme is most likely active, as its amino acid sequence is 73% identical and 84% similar to that of EcDHPS. Of the residues in contact with the substrates, 18 are conserved in the highly active DHPSs and also in the very sluggish FtHPPK-DHPS (Fig. 7). Because FtHPPK-DHPS has a very high K_m value for *p*ABA (Table 3), its low DHPS activity is probably due to non-conserved active site residues that interact with this substrate. Indeed, an αloop7 residue that interacts with the carboxylate anion of *p*ABA, which likely plays a role of anchoring the substrate in the active site, is not conserved. This residue is a serine in BaDHPS, EcDHPS, and YpDHPS; an arginine in MtDHPS1, SaDHPS, and SpDHPS; a lysine in ScDHPS; an aspartate in MtDHPS2; and a proline in FtHPPK-DHPS (Fig. 7). The serine residue in YpDHPS forms a hydrogen bond with the carboxylate of *p*ABA [34], the arginine or lysine in MtDHPS1, SaDHPS, ScDHPS, and SpDHPS has the potential to form a hydrogen bond with the carboxylate, but the proline (P383) in FtHPPK-DHPS cannot form a hydrogen bond with the carboxylate (Fig. 9A). Furthermore, the adjacent serine residue (S384) also cannot

form such a hydrogen bond (Fig. 9B). This αloop7 residue is an aspartate in MtDHPS2, which is at least partially responsible for the lack of DHPS activity, as the interaction between two carboxylate anions is repulsive. The inactivity of MtDHPS2 may be also due to the replacement of three conserved active site residues (Ser-Thr-Arg) in loop2 by Lys-Ala-Gly. The αloop7 is important for binding both substrates; it contains many mutations that cause resistance to sulfa drugs (Fig. 7). The conformation of this loop in FtHPPK-DHPS is, however, significantly different from those in the more active DHPSs, including YpDHPS [34] (Fig. 9B), most likely because of two proline substitutions, one at the beginning and the other in the middle of the loop (Fig. 7). Another notable difference between FtDHPS and other DHPSs is the C-terminal truncation in FtDHPS (Fig. 7), which removes the C-terminal helix present in other DHPSs. However, this truncation may not be functionally significant, as none of the residues in this helix are in contact with the substrates. The C-terminal helix may play a structural role in stabilizing the enzyme, rather than a functional role in catalysis. Whether the αloop7 substitutions and the C-terminal truncation are responsible for the low DHPS activity can be tested by site-directed mutagenesis studies.

Sulfa drugs are not recommended for the treatment of tularemia because they are ineffective against this disease [40]. This inefficacy could be due to their low inhibitory activities against FtHPPK-DHPS, resulting from the structural differences between the *p*ABA-binding pocket of FtHPPK-DHPS and those of active DHPSs. Another possibility is that *F. tularensis* is able to uptake folates from host cells and is not reliant on *de novo* folate biosynthesis. These possibilities can be tested experimentally by sulfonamide inhibition measurements, and folate biosynthesis and uptake experiments using normal and folate-depleted host cells.

FtHPPK-DHPS as an attractive target for the development of tularemia therapeutics

M. tuberculosis has two DHPS genes. While MtDHPS2 is inactive, the catalytic efficiency of MtDHPS1 is comparable to those of other highly active DHPSs such as EcDHPS and BaDHPS (Table 3). Unlike *M. tuberculosis*, a BLAST search of the sequenced genomes of 10 *F. tularensis* strains using the DHPS sequence of FtHPPK-DHPS found only one gene in each genome. Hence, it is surprising that FtHPPK-DHPS has such a low DHPS activity. It is also intriguing because the marginal DHPS activity of FtHPPK-DHPS makes this enzyme very attractive as a target for developing new sulfa drugs for the treatment of tularemia. We believe that the marginal DHPS activity makes *F. tularensis* more vulnerable to inhibition by effective DHPS inhibitors.

The evolution of antibiotic resistance by mutation usually exacts a toll on the fitness of the microorganism, the magnitude of which is the main determinant for the rate at which resistance develops [41]. With respect to an enzyme target, the reduction in fitness may be manifested by a decrease in its catalytic efficiency. For example, the P64S mutation in loop2 of EcDHPS causes a 100-fold increase in the K_i value for the sulfa drug sulfathiazole but also a tenfold increase in the K_m value for the substrate *p*ABA, resulting in a less efficient enzyme [42]. Considering the very low catalytic efficiency of wild-type FtHPPK-DHPS, any mutation that further reduces its DHPS activity may be lethal to *F. tularensis*. We believe that it will be difficult for *F. tularensis* to develop resistance to effective DHPS inhibitors.

The sluggishness of the DHPS activity of the tested FtHPPK-DHPS enzyme also raises two significant issues that need to be addressed in further studies. First, is the sluggishness of the DHPS activity a unique property of the tested enzyme or a common property of all FtHPPK-DHPS enzymes? In the UniProtKB database (http://www.uniprot.org/), currently there are 39 HPPK-DHPSs that belong to the genus *Francisella*, of which 34 belong to the species *Francisella tularensis*. These enzymes are highly conserved. The amino acid sequence identities between the 39 *Francisella* HPPK-DHPS enzymes are high, ranging 78–100%. Of the 34 HPPK-DHPS enzymes that belong to *F. tularensis*, 17 are identical, 10 have a sequence identity of 99%, and seven have a sequence identity of 94–97% (Fig. S1). All *Francisella* HPPK-DHPS enzymes do not have the C-terminal helix present in other DHPSs. The amino acid sequences of αloop7 involved in binding *p*ABA are identical for all but one *Francisella* HPPK-DHPS enzyme. The latter enzyme has a 99% sequence identity to the tested FtHPPK-DHPS but has one substitution in αloop7, with a Pro replaced with a Gln (Fig. S1). Whether the Gln residue can form a hydrogen bond with the carboxylate of *p*ABA is not clear. If the αloop7 of this FtHPPK-DHPS assumes the conformation revealed by the crystal structures, the Gln residue may not be able to form a hydrogen bond with the substrate *p*ABA. Based on the very high sequence conservation described above, the sluggishness of the DHPS activity is likely shared by most, if not all, FtHPPK-DHPS enzymes. Furthermore, the very high sequence conservation also suggests that the DHPS activity is important for the growth of *F. tularensis*, which leads to the second question: Can the sluggish DHPS activity of FtHPPK-DHPS support the growth of *F. tularensis*? It has been shown that *F. tularensis* can grow in a chemically defined synthetic medium without folate [43]. However, *F. tularensis* may grow faster in the cells of a living animal or human being. Whether FtHPPK-DHPS can support the growth of *F. tularensis* inside the host needs to be tested using folate-depleted host cells.

The clinical use of sulfa drugs marked the beginning of the modern era of antibiotic treatment of infectious diseases [44]. Sulfa drugs are a class of least expensive antibiotics and remain in clinical use [6], particularly for the treatment of pneumocystis pneumonia, for which the sulfa drug sulfamethoxazole in combination with trimethoprim is the preferred regimen for treatment and prophylaxis [45]. However, the development of resistance has severely limited the clinical use of sulfa drugs [6]. Because the reaction catalyzed by HPPK is coupled to that catalyzed by DHPS, inhibitors of the two enzymes should have a synergistic effect on microbial growth. Therefore, it is advantageous to develop inhibitors against both activities of the bifunctional enzyme *F. tularensis*. Our work suggests that it is highly feasible to design potent inhibitors of FtHPPK-DHPS and the structural and functional data are essential for the development of new tularemia therapeutics.

Experimental Procedures

Cloning, protein expression and purification of FtHPPK-DHPS

The open reading frame encoding HPPK-DHPS was cloned from *F. tularensis* SCHU S4 genomic DNA (a gift from Dr. Robert Ulrich, United States Army Medical Research Institute of Infectious Diseases) with primers p48-HPPKf (5'-GAGAACCTGTACTTCCAGGGTATGCAATATATTATAGGAATTGG-3') and p49-HPPKr

(5'-GGGGACCACTTTGTACAAGAAAGCTGGGTTATTAAATCTTGTGTACTCTTATAATATC-3') using KOD Hot Start DNA polymerase (Novagen-EMD Millipore, Billerica, MA). The PCR product was gel purified and used as the template for a second PCR with primers PE-277 (5'-GGGGACAAGTTTGTACAAAAAAGCAGGCTCGGAGAACCTGTACTTCCAG-3') and p49-HPPKr. This amplicon was inserted into pDONR201 by Gateway recombinational cloning (Life Technologies, Grand Island, NY) to generate entry clone pZD46. The entry clone was then recombined with destination vector pDEST-HisMBP [46] to construct the His_6-MBP-HPPK-DHPS fusion protein expression vector pZD47, with a recognition site for tobacco etch virus (TEV) protease between the MBP and HPPK domains. Because this fusion protein proved difficult to cleave with TEV protease, two additional glycine residues were added between the TEV site and the N-terminus of HPPK by QuikChange mutagenesis (Agilent Technologies, Santa Clara, CA) to generate pDN2163. The fusion protein was expressed in the *E. coli* strain BL21-CodonPlus(DE3)-RIL (Agilent Technologies, Santa Clara, CA). Cells containing the expression plasmid were grown to mid-log phase (OD_{600} ~ 0.5) at 37°C in LB broth containing 100 μg ml^{-1} ampicillin, 30 μg ml^{-1} chloramphenicol and 0.2% glucose. Overproduction of fusion protein was induced with isopropyl-β-D-thiogalactopyranoside at a final concentration of 1 mM for 4 h at 30°C. The cells were pelleted by centrifugation and stored at −80°C.

All purification procedures were performed at 4–8°C. *E. coli* cell paste was suspended in ice-cold 25 mM HEPES (pH 7.5), 100 mM NaCl, 10% glycerol, 25 mM imidazole buffer (buffer A) containing Complete EDTA-free protease inhibitor cocktail tablets (Roche Molecular Biochemicals, Indianapolis, IN). The cells were lysed with an APV-1000 homogenizer (Invensys APV Products, Albertslund, Denmark) at ~10,000 psi, and centrifuged at 30,000 × *g* for 30 min. The supernatant was filtered through a 0.45 μm polyethersulfone membrane and applied to a Ni-NTA superflow column (Qiagen, Valencia, CA) equilibrated in buffer A. The column was washed to baseline with buffer A and eluted with a linear gradient of imidazole to 250 mM. Fractions containing recombinant His_6-MBP-HPPK-DHPS fusion protein were pooled, concentrated using an Amicon Ultracel® 30 KDa cellulose membrane (EMD Millipore Corporation, Billerica, MA), diluted with 25 mM HEPES (pH 7.5), 100 mM NaCl, 10% glycerol buffer to reduce the imidazole concentration to about 25 mM, and digested overnight at 4°C with His_6-tagged TEV protease [47]. The digest was applied to a second Ni-NTA superflow column equilibrated in buffer A and recombinant protein emerged in the column effluent. The effluent was incubated overnight with dithiothreitol (10 mM), concentrated using an Amicon Ultracel® 10 KDa cellulose membrane, and applied to a HiPrep 26/60 Sephacryl S-200 HR column (GE Healthcare Bio-Sciences Corporation, Piscataway, NJ) equilibrated in 25 mM HEPES (pH 7.5), 150 mM NaCl, 10% glycerol, 2 mM tris(2-carboxyethyl) phosphine buffer. The peak fractions containing HPPK-DHPS were pooled and concentrated to 13–14 mg ml^{-1} (estimated at 280 nm using a molar extinction coefficient of 43890 M^{-1} cm^{-1} derived using the Expasy ProtParam tool) [48]. Recombinant protein was used immediately or flash-frozen in liquid nitrogen and stored at −80°C. The final product was judged to be >95% pure by sodium

dodecyl sulfate-polyacrylamide gel electrophoresis. The molecular weight was confirmed by electrospray ionization mass spectrometry.

Biochemical methods

EcHPPK and EcDHPS were prepared as described [19, 49]. IC_{50} measurements of the bisubstrate inhibitors for FtHPPK-DHPS were carried out as described [14–16]. The only differences are components and concentrations in the initial reaction mixtures, which contained 10 nM FtHPPK-DHPS, 5 μM ATP, 2 μM HP, 5 mM $MgCl_2$, 25 mM DTT, various concentrations of an inhibitor, and a trace amount of [α-^{32}P]-ATP (~1 μCi) in 100 mM Tris-HCl (pH 8.3). IC_{50} values were obtained by fitting the data to equation 1 by nonlinear least-squares regression.

$$v = v_{\min} + (v_{\max} - v_{\min})/(1 + [\mathrm{I}]/\mathrm{IC}_{50}) \quad \text{(eq. 1)}$$

where v is the observed reaction rate, $v_{\min}$ the minimum reaction rate, $v_{\max}$ the maximum reaction rate, and [I] the concentration of the inhibitor. The K_i values were calculated from the IC_{50} values using the Cheng-Prusoff equation [27, 28].

$$K_i = \mathrm{IC}_{50}/(1 + [\mathrm{S}]/K_m) \quad \text{(eq. 2)}$$

K_d value for HP-26 binding to FtHPPK was determined using fluorometry as previously described [16].

The kinetic constants for HPPK activity were determined by measuring the conversion of ATP to AMP using [α-^{32}P]-ATP or the conversion of HP to HPPP using DHPS as a coupling enzyme and [7–^{14}C]-*p*ABA as previously described [21]. In the direct kinetic assay of the HPPK activity of FtHPPK-DHPS, the reaction mixture contained 10 nM FtHPPK-DHPS, 10 mM $MgCl_2$, 25 mM DTT, and various concentrations of ATP or HP with the other HPPK substrate fixed. The reaction was stopped by the addition of 1/5 reaction volume of 500 mM EDTA and the reaction mixture separated by thin-layer chromatography on a plastic sheet coated with PEI-cellulose. In the coupling assay for measuring the kinetic constants of EcHPPK, the initial reaction mixture in 100 mM Tris-HCl (pH 8.3) contained 1 nM EcHPPK, 11 μM EcDHPS, 20 μM *p*ABA, 10 mM $MgCl_2$, 25 mM DTT, and various concentrations of ATP or HP with the other HPPK substrate fixed. In the coupling assay for measuring the kinetic constants of the HPPK activity of FtHPPK-DHPS, the initial reaction mixture contained 10 nM FtHPPK-DHPS, 10 μM EcDHPS, 10 μM *p*ABA, 10 mM $MgCl_2$, 25 mM DTT, and various concentrations of ATP or HP. The reaction was stopped by the addition of 1/5 reaction volume of a solution containing 1.2 M acetic acid and 18 mM unlabeled *p*ABA and the reaction mixture separated by paper chromatography using Whatman 3MM chromatography paper. For measuring the kinetic constants of the DHPS activity, the reaction mixture in 100 mM Tris-HCl (pH 8.3) contained 1 μM EcHPPK, 10 μM FtHPPK-DHPS, 1 mM ATP, 5 mM $MgCl_2$, 100 μM HP, 1 mM TCEP, and various concentrations of *p*ABA. The substrate HPPP was generated in situ with EcHPPK, and the DHPS reaction was initiated with the addition of FtHPPK-DHPS. The reaction was stopped

and the reaction mixture separated as described above for the coupling assay. The radioactivities of separated compounds were quantified by a Molecular Dynamics Storm 820 PhosphorImager. The kinetic parameters were obtained by nonlinear fitting of the initial velocity data to the standard Michaelis-Menten equation using the Origin program. All standard deviations were calculated from the values of repeated experiments.

Crystallization, X-ray diffraction, structure solution and refinement

The Hydra II Plus One crystallization robot (Matrix Technologies, Hudson, New Hampshire, USA) and Crystal Screen kits from Hampton Research (Laguna Niguel, California, USA) were used. Crystals were grown at 19±1°C in sitting drops containing 0.3 μl protein solution and 0.3 μl well solution. The protein solution contained 11 mg/mL FtHPPK-DHPS, saturated HP-26, 150 mM NaCl, 10% glycerol, and 2 mM TCEP in 25 mM HEPES (pH 7.5), and the well solution contained 28% (w/v) PEG monomethyl ether 2000 in 100 mM Bis-Tris (pH 6.5). The cryoprotectant contained 75% (v/v) well solution and 25% (v/v) ethylene glycol. X-ray diffraction data were collected at 100K with an MARCCD detector mounted at the synchrotron Beamline BL9-2 at the Stanford Synchrotron Radiation Lightsource. Data processing was carried out with HKL2000 [50]. The statistics of the diffraction data are summarized in Table 2.

We solved the FtHPPK-DHPS•HP-26 structure by molecular replacement. The search models were the EcHPPK•HP-18 and BaDHPS structures (PDB entries 3UDE and 1TWS) [16, 51]. Structure solution and refinement were done with PHENIX [52]. The rotation and translation function Z-scores for the HPPK domain were 5.8 and 4.9, respectively, and the Z-scores for the DHPS domain were 4.1 and 8.9, respectively. There were seven packing clashes in the initial model, of which the R-free and R-work values were 0.46 and 0.39, respectively. All graphics work, including model building and rebuilding, was performed with COOT [53]. The structures were verified with annealed omit maps and the geometry was assessed using PROCHECK [54] and WHAT IF [55]. The statistics of the crystal structure are summarized in Table 2. Illustrations were prepared with PyMOL [56].

Supplementary Material

Refer to Web version on PubMed Central for supplementary material.

Acknowledgments

Mass spectrometry experiments were conducted on an Agilent 1100 series LC/Mass Selective Detector maintained by the Biophysics Resource in the Structural Biophysics Laboratory of National Cancer Institute at Frederick. X-ray diffraction data were collected at the Stanford Synchrotron Radiation Lightsource. This research was supported by the Intramural Research Program of the NIH, National Cancer Institute, Center for Cancer Research (X.J.) and NIH grant R01GM084402 (H.Y.).

Abbreviations

DHNA	dihydroneopterin aldolase
HPPK	6-hydroxymethyl-7,8-dihydropterin pyrophosphokinase
DHPS	dihydropteroate synthase

DHFS	dihydrofolate synthase
HP	6-hydroxymethyl-7,8-dihydropterin
HPPP	6-hydroxymethyl-7,8-dihydropterin pyrophosphate
***p*ABA**	*p*-aminobenzoic acid
PP	pyrophosphate ion
XHP	2-amino-6-methylidene-6,7-dihydropterindin-4(3H)-one
HP-18	5'-S-[1-(2-{[(2-amino-7,7-dimethyl-4-oxo-3-4,7,8-tetrahydropteridin-6-yl)carbonyl]amino}ethyl)piperidin-4-yl]-5'-thioadenosine
HP-26	2-amino-7,7-dimethyl-4-oxo-3,4,7,8-tetrahydro-pteridine-6-carboxylic acid (2-{2-[5-(6-amino-purin-9-yl)-3,4-dihydroxy-tetrahydro-furan-2-ylmethanesulfonyl]-ethylcarbamoyl}-ethyl)-amide
PDB	Protein Data Bank
RMSD	root-mean-square deviation

References

1. Bermingham A, Derrick JP. The folic acid biosynthesis pathway in bacteria: evaluation of potential for antibacterial drug discovery. Bioessays. 2002; 24:637–648. [PubMed: 12111724]
2. Walsh C. Where will new antibiotics come from? Nat Rev Microbiol. 2003; 1:65–70. [PubMed: 15040181]
3. Hitchings GH, Burchall JJ. Inhibition of folate biosynthesis and function as a basis for chemotherapy. Adv Enzymol Relat Areas Mol Biol. 1965; 27:417–468. [PubMed: 4387360]
4. Hughes, DTD. Chapter 17. Diaminopyrimidines. In: O'Grady, F.Lambert, HP.Finch, RG., Greenwood, D., editors. Antibiotics and Chemotherapy. Churchill Livingstone; New York: 2010.
5. Hughes, DTD. Chapter 29. Sulphonamides. In: O'Grady, F.Lambert, HP.Finch, RG., Greenwood, D., editors. Antibiotics and Chemotherapy. Churchill Livingstone; New York: 2010.
6. Zinner, SH., Mayer, KH. Sulfonamides and trimethoprim. In: Mandell, GL.Bennett, JE., Dolin, R., editors. Principles and Practice of Infectious Diseases. Churchill Livingstone; Philadelphia: 2009. p. 475-485.
7. Lawrence MC, Iliades P, Fernley RT, Berglez J, Pilling PA, Macreadie IG. The three-dimensional structure of the bifunctional 6-hydroxymethyl-7,8-dihydropterin pyrophosphokinase/dihydropteroate synthase of Saccharomyces cerevisiae. J Mol Biol. 2005; 348:655–670. [PubMed: 15826662]
8. Derrick, JP. The structure and mechanism of 6-hydroxymethyl-7,8-dihydropterin pyrophosphokinase. In: Litwack, G., editor. Folic Acid and Folates. Academic Press; Oxford, UK: 2008. p. 411-433.
9. Yan H, Ji X. Role of protein conformational dynamics in the catalysis by 6-hydroxymethyl-7,8-dihydropterin pyrophosphokinase. Protein Pept Lett. 2011; 18:328–335. [PubMed: 21222642]
10. Wood, HCS. Specific inhibition of dihydrofolate biosynthesis - a new approach to chemoherapy. In: Pfleiderer, W., editor. Chemistry and Biology of Pteridines. Walter de Gruyter; Berlin-New York: 1975.
11. Al-Hassan SS, Cameron RJ, Curran AWC, Lyall WJS, Nicholson SH, Robinson DR, Stuart A, Suckling CJ, Stirling I, Wood HCS. Specific inhibitors in vitamin biosynthesis. Part 7. Syntheses of blocked 7, 8-dihydropteridines via -amino ketones. J Chem Soc, Perkin Trans. 1985; 1:1645–1659.

12. Hennig M, Dale GE, D'Arcy A, Danel F, Fischer S, Gray CP, Jolidon S, Muller F, Page MG, Pattison P, et al. The structure and function of the 6-hydroxymethyl-7,8-dihydropterin pyrophosphokinase from *Haemophilus influenzae*. J Mol Biol. 1999; 287:211–219. [PubMed: 10080886]

13. Stammers DK, Achari A, Somers DO, Bryant PK, Rosemond J, Scott DL, Champness JN. 2.0 Å X-ray structure of the ternary complex of 7,8-dihydro-6-hydroxymethylpterinpyrophosphokinase from Escherichia coli with ATP and a substrate analogue. FEBS Lett. 1999; 456:49–53. [PubMed: 10452528]

14. Shi G, Blaszczyk J, Ji X, Yan H. Bisubstrate analogue inhibitors of 6-hydroxymethyl-7,8-dihydropterin pyrophosphokinase: synthesis and biochemical and crystallographic studies. J Med Chem. 2001; 44:1364–1371. [PubMed: 11311059]

15. Shi G, Shaw G, Li Y, Wu Y, Yan H, Ji X. Bisubstrate analog inhibitors of 6-hydroxymethyl-7,8-dihydropterin pyrophosphokinase: New lead exhibits a distinct binding mode. Bioorg Med Chem. 2012; 20:4303–4309. [PubMed: 22727779]

16. Shi G, Shaw G, Liang YH, Subburaman P, Li Y, Wu Y, Yan H, Ji X. Bisubstrate analogue inhibitors of 6-hydroxymethyl-7,8-dihydropterin pyrophosphokinase: New design with improved properties. Bioorg Med Chem. 2012; 20:47–57. [PubMed: 22169600]

17. Shiota, T. Biosynthesis of folate from pterin precursors. In: Blakley, RT., Benkovic, SJ., editors. Chemistry and Biochemistry of Folates. John Wiley & Sons; New York: 1984. p. 121-134.

18. Blaszczyk J, Shi G, Li Y, Yan H, Ji X. Reaction trajectory of pyrophosphoryl transfer catalyzed by 6-hydroxymethyl-7,8-dihydropterin pyrophosphokinase. Structure (Camb). 2004; 12:467–475. [PubMed: 15016362]

19. Shi G, Gong Y, Savchenko A, Zeikus JG, Xiao B, Ji X, Yan H. Dissecting the nucleotide binding properties of Escherichia coli 6-hydroxymethyl-7,8-dihydropterin pyrophosphokinase with fluorescent 3'(2)'-o-anthraniloyladenosine 5'-triphosphate. Biochim Biophys Acta. 2000; 1478:289–299. [PubMed: 10825540]

20. Bermingham A, Bottomley JR, Primrose WU, Derrick JP. Equilibrium and kinetic studies of substrate binding to 6-hydroxymethyl-7,8-dihydropterin pyrophosphokinase from *Escherichia coli*. J Biol Chem. 2000; 275:17962–17967. [PubMed: 10751386]

21. Li Y, Gong Y, Shi G, Blaszczyk J, Ji X, Yan H. Chemical transformation is not rate-limiting in the reaction catalyzed by *Escherichia coli* 6-hydroxymethyl-7,8-dihydropterin pyrophosphokinase. Biochemistry. 2002; 41:8777–8783. [PubMed: 12093297]

22. Blaszczyk J, Shi G, Yan H, Ji X. Catalytic center assembly of HPPK as revealed by the crystal structure of a ternary complex at 1.25 Å resolution. Structure. 2000; 8:1049–1058. [PubMed: 11080626]

23. Moran GJ, Krishnadasan A, Gorwitz RJ, Fosheim GE, McDougal LK, Carey RB, Talan DA. Methicillin-resistant *S. aureus* infections among patients in the emergency department. N Engl J Med. 2006; 355:666–674. [PubMed: 16914702]

24. Kaplan JE, Benson C, Holmes KK, Brooks JT, Pau A, Masur H. Guidelines for prevention and treatment of opportunistic infections in HIV-infected adults and adolescents: recommendations from CDC, the National Institutes of Health, and the HIV Medicine Association of the Infectious Diseases Society of America. MMWR Recomm Rep. 2009; 58:1–207. quiz CE201-204.

25. Hevener KE, Yun MK, Qi J, Kerr ID, Babaoglu K, Hurdle JG, Balakrishna K, White SW, Lee RE. Structural studies of pterin-based inhibitors of dihydropteroate synthase. J Med Chem. 2010; 53:166–177. [PubMed: 19899766]

26. Pemble CW IV, Mehta PK, Mehra S, Li Z, Nourse A, Lee RE, White SW. Crystal structure of the 6-hydroxymethyl-7,8-dihydropterin pyrophosphokinase:dihydropteroate synthase bifunctional enzyme from *Francisella tularensis*. PloS one. 2010; 5:e14165. [PubMed: 21152407]

27. Cheng YC, Prussof WH. Relationship between the inhibition constant (K_i) and the concentration of inhibitor which causes 50 per cent inhibition (I_{50}) of an enzymatic reaction. Biochem Pharmacol. 1973; 22:3099–3108. [PubMed: 4202581]

28. Cer RZ, Mudunuri U, Stephens R, Lebeda FJ. IC_{50}-to-K_i: a web-based tool for converting IC_{50} to K_i values for inhibitors of enzyme activity and ligand binding. Nucleic Acids Res. 2009; 37:W441–445. [PubMed: 19395593]

29. Xiao B, Shi G, Gao J, Blaszczyk J, Liu Q, Ji X, Yan H. Unusual conformational changes in 6-hydroxymethyl-7,8-dihydropterin pyrophosphokinase as revealed by X-ray crystallography and NMR. J Biol Chem. 2001; 276:40274–40281. [PubMed: 11546767]
30. Blaszczyk J, Li Y, Wu Y, Shi G, Ji X, Yan H. Essential roles of a dynamic loop in the catalysis of 6-hydroxymethyl-7,8-dihydropterin pyrophosphokinase. Biochemistry. 2004; 43:1469–1477. [PubMed: 14769023]
31. Blaszczyk J, Li Y, Shi G, Yan H, Ji X. Dynamic Roles of Arginine Residues 82 and 92 of *Escherichia coli* 6-Hydroxymethyl-7,8-dihydropterin Pyrophosphokinase: Crystallographic Studies. Biochemistry. 2003; 42:1573–1580. [PubMed: 12578370]
32. Li Y, Wu Y, Blaszczyk J, Ji X, Yan H. Catalytic Roles of Arginine Residues 82 and 92 of *Escherichia coli* 6-Hydroxymethyl-7,8-dihydropterin Pyrophosphokinase: Site-Directed Mutagenesis and Biochemical Studies. Biochemistry. 2003; 42:1581–1588. [PubMed: 12578371]
33. Talarico TL, Dev IK, Dallas WS, Ferone R, Ray PH. Purification and partial characterization of 7,8-dihydro-6-hydroxymethylpterin-pyrophosphokinase and 7,8-dihydropteroate synthase from Escherichia coli MC4100. J Bacteriol. 1991; 173:7029–7032. [PubMed: 1657875]
34. Yun MK, Wu Y, Li Z, Zhao Y, Waddell MB, Ferreira AM, Lee RE, Bashford D, White SW. Catalysis and sulfa drug resistance in dihydropteroate synthase. Science. 2012; 335:1110–1114. [PubMed: 22383850]
35. Nopponpunth V, Sirawaraporn W, Greene PJ, Santi DV. Cloning and expression of Mycobacterium tuberculosis and Mycobacterium leprae dihydropteroate synthase in Escherichia coli. J Bacteriol. 1999; 181:6814–6821. [PubMed: 10542185]
36. Hennig M, D'Arcy A, Hampele IC, Page MG, Oefner C, Dale GE. Crystal structure and reaction mechanism of 7,8-dihydroneopterin aldolase from Staphylococcus aureus. Nat Struct Biol. 1998; 5:357–362. [PubMed: 9586996]
37. Berglez J, Pilling P, Macreadie I, Fernley RT. Purification, properties, and crystallization of Saccharomyces cerevisiae dihydropterin pyrophosphokinase-dihydropteroate synthase. Protein Expr Purif. 2005; 41:355–362. [PubMed: 15866722]
38. Garçon A, Levy C, Derrick JP. Crystal structure of the bifunctional dihydroneopterin aldolase/6-hydroxymethyl-7,8-dihydropterin pyrophosphokinase from *Streptococcus pneumoniae*. J Mol Biol. 2006; 360:644–653. [PubMed: 16781731]
39. Gengenbacher M, Xu T, Niyomrattanakit P, Spraggon G, Dick T. Biochemical and structural characterization of the putative dihydropteroate synthase ortholog Rv1207 of Mycobacterium tuberculosis. FEMS Microbiol Lett. 2008; 287:128–135. [PubMed: 18680522]
40. Harik NS. Tularemia: epidemiology, diagnosis, and treatment. Pediatr Ann. 2013; 42:288–292. [PubMed: 23805970]
41. Andersson DI, Hughes D. Antibiotic resistance and its cost: is it possible to reverse resistance? Nat Rev Microbiol. 2010; 8:260–271. [PubMed: 20208551]
42. Vedantam G, Nichols BP. Characterization of a mutationally altered dihydropteroate synthase contributing to sulfathiazole resistance in Escherichia coli. Microb Drug Resist. 1998; 4:91–97. [PubMed: 9650994]
43. Chamberlain RE. Evaluation of Live Tularemia Vaccine Prepared in a Chemically Defined Medium. Appl Microbiol. 1965; 13:232–235. [PubMed: 14325885]
44. Wainwright M, Kristiansen JE. On the 75th anniversary of Prontosil. Dyes Pigments. 2011; 88:231–234.
45. Walzer, PD., Smulian, AG. Sulfonamides and trimethoprim. In: Mandell, GL.Bennett, JE., Dolin, R., editors. Principles and Practice of Infectious Diseases. Churchill Livingstone; Philadelphia: 2009. p. 3377-3399.
46. Nallamsetty S, Austin BP, Penrose KJ, Waugh DS. Gateway vectors for the production of combinatorially-tagged His6-MBP fusion proteins in the cytoplasm and periplasm of Escherichia coli. Protein Sci. 2005; 14:2964–2971. [PubMed: 16322578]
47. Kapust RB, Tözsér J, Fox JD, Anderson DE, Cherry S, Copeland TD, Waugh DS. Tobacco etch virus protease: mechanism of autolysis and rational design of stable mutants with wild-type catalytic proficiency. Protein Eng. 2001; 14:993–1000. [PubMed: 11809930]

48. Gasteiger, E., Hoogland, C., Gattiker, A., Duvaud, S., Wilkins, MR., Appel, RD., Bairoch, A. Protein Identification and Analysis Tools on the ExPASy Server. In: Walker, JM., editor. The Proteomics Protocols Handbook. Humana Press; 2005. p. 571-607.

49. Dallas WS, Gowen JE, Ray PH, Cox MJ, Dev IK. Cloning, sequencing, and enhanced expression of the dihydropteroate synthase gene of Escherichia coli MC4100. J Bacteriol. 1992; 174:5961–5970. [PubMed: 1522070]

50. Otwinowski Z, Minor W. Processing of X-ray diffraction data collected in oscillation mode. Methods Enzymol. 1997; 276:307–326.

51. Babaoglu K, Qi J, Lee RE, White SW. Crystal structure of 7,8-dihydropteroate synthase from Bacillus anthracis: Mechanism and novel inhibitor design. Structure. 2004; 12:1705–1717. [PubMed: 15341734]

52. Adams PD, Grosse-Kunstleve RW, Hung LW, Ioerger TR, McCoy AJ, Moriarty NW, Read RJ, Sacchettini JC, Sauter NK, Terwilliger TC. PHENIX: Building new software for automated crystallographic structure determination. Acta Crystallogr D. 2002; 58:1948–1954. [PubMed: 12393927]

53. Emsley P, Cowtan K. Coot: model-building tools for molecular graphics. Acta Crystallogr D. 2004; 60:2126–2132. [PubMed: 15572765]

54. Laskowski RA, MacArthur MW, Moss DS, Thornton JM. PROCHECK: a program to check the stereochemical quality of protein structures. J Appl Crystallog. 1993; 26:283–291.

55. Vriend G. WHAT IF: a molecular modeling and drug design program. J Mol Graph. 1990; 8:52–56. 29. [PubMed: 2268628]

56. DeLano, WL. The PyMOL Molecular Graphics System. Delano Scientific; San Carlos, CA: 2002. The PyMOL Molecular Graphics System.

57. Lovell SC, Davis IW, Arendall WB 3rd, de Bakker PI, Word JM, Prisant MG, Richardson JS, Richardson DC. Structure validation by Calpha geometry: phi,psi and Cbeta deviation. Proteins: Struct Funct Genet. 2003; 50:437–450. [PubMed: 12557186]

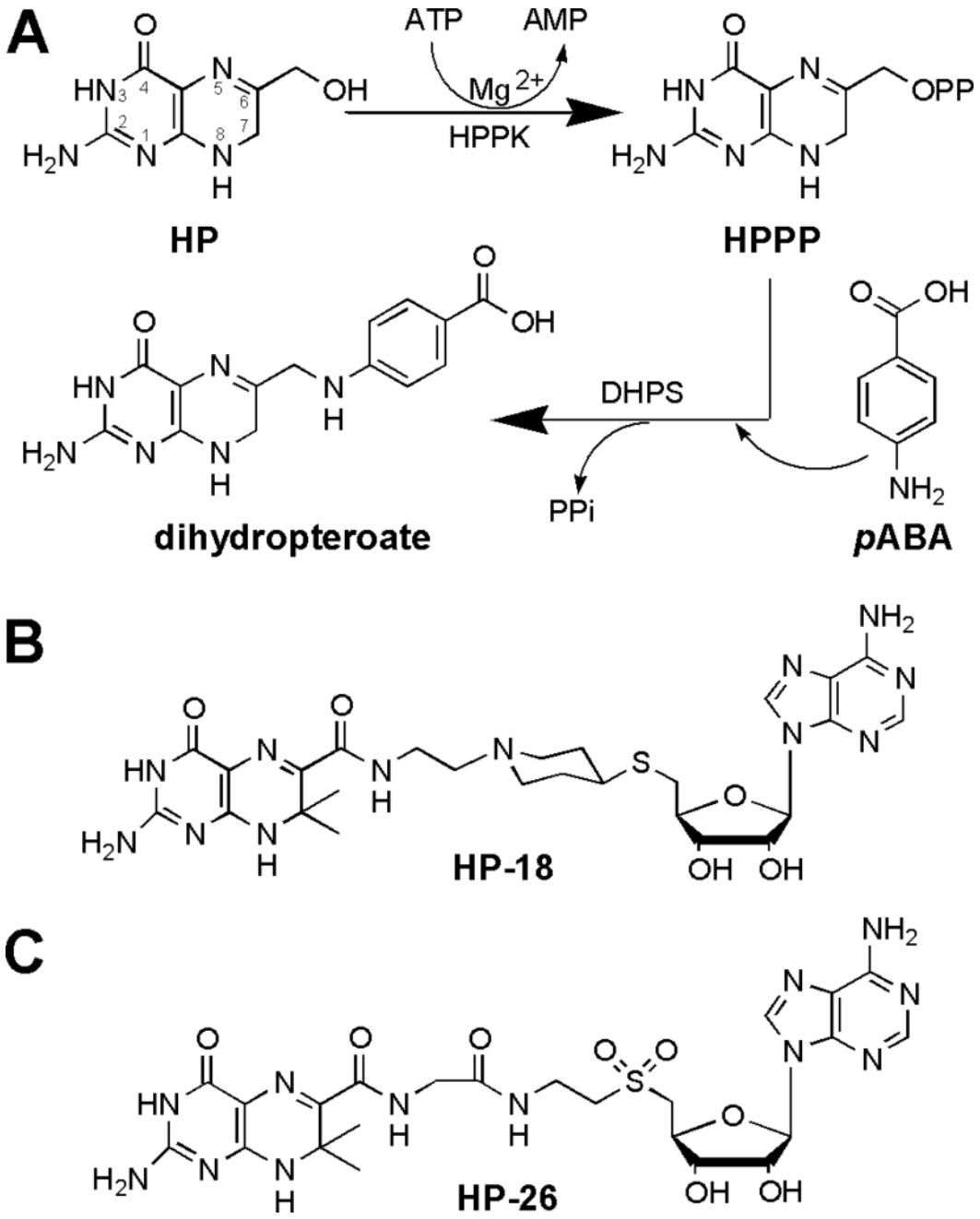

Figure 1.

HPPK- and DHPS-catalyzed reactions and bisubstrate analogue inhibitors of HPPK. (A) The chemical structures of the substrates and products of HPPK- and DHPS-catalyzed reactions. (B) Chemical structure of HP-18 [16]. (C) Chemical structure of HP-26 [15].

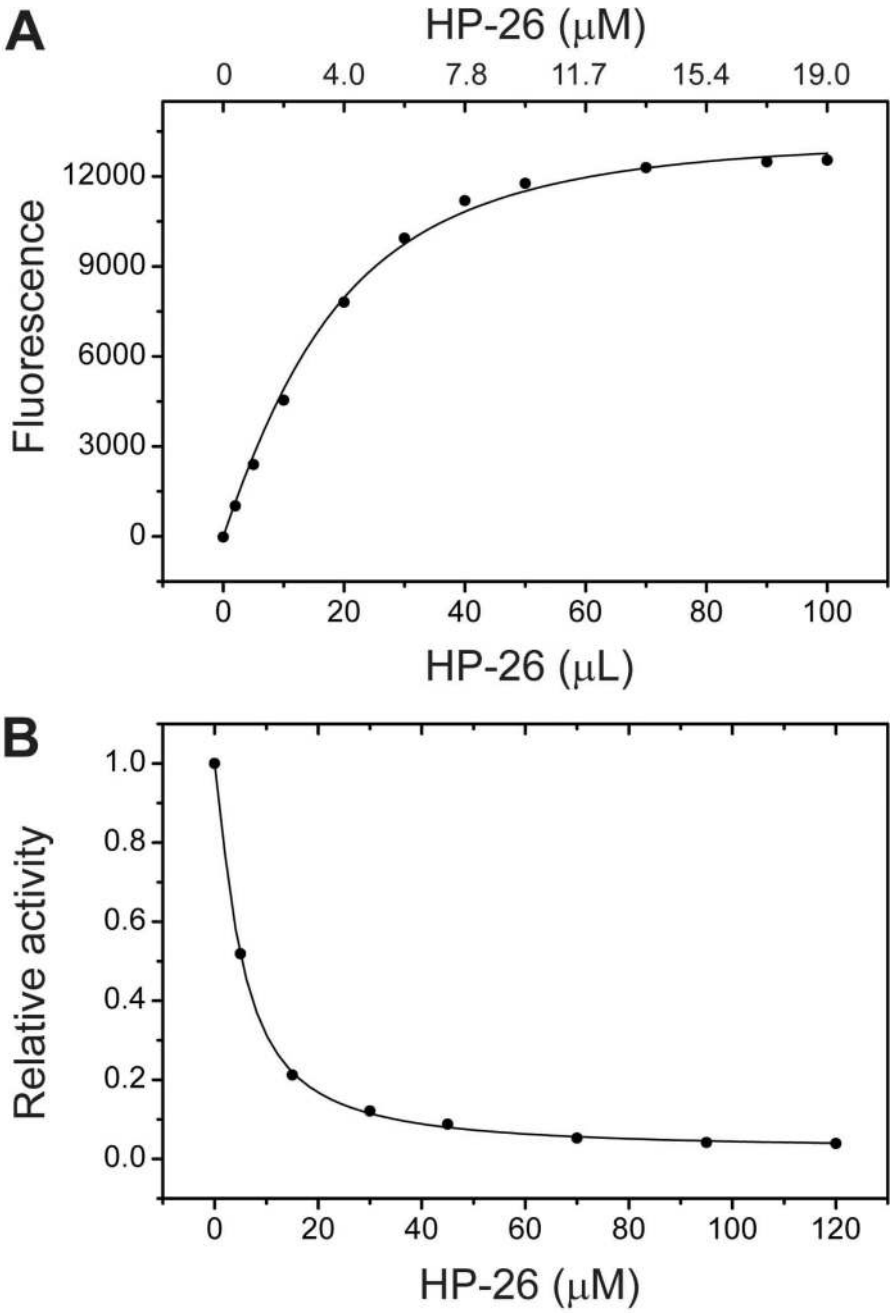

Figure 2.

K_d and IC_{50} measurements. (A) Fluorometric titration of HPPK with HP-26. (B) Inhibition of HPPK by HP-26.

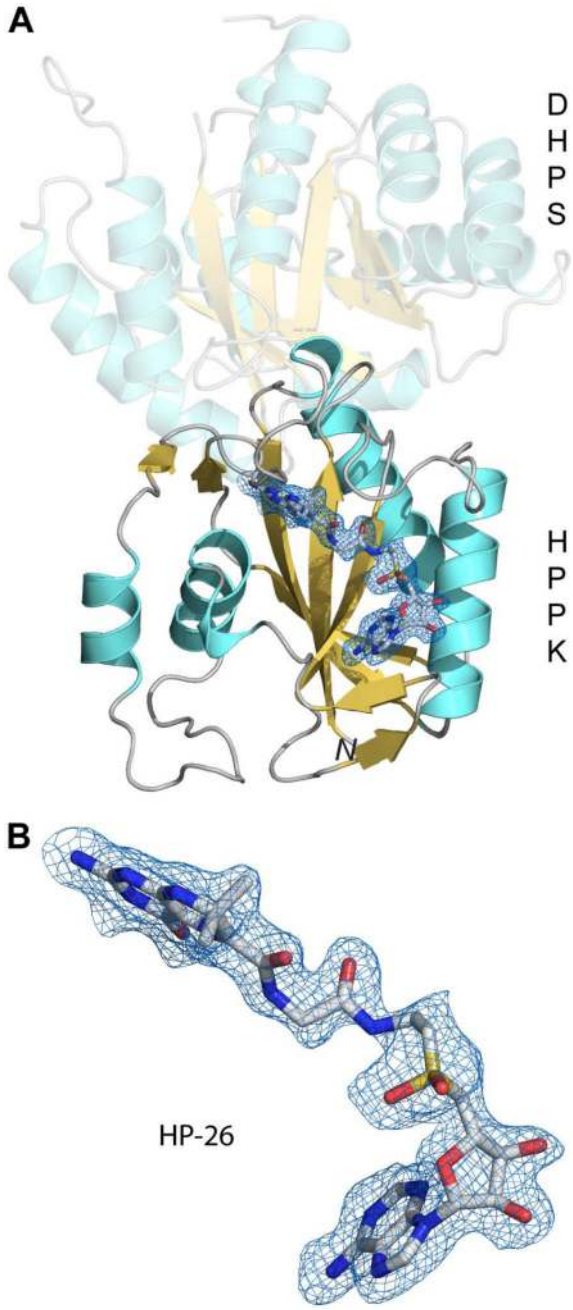

Figure 3.

The FtHPPK-DHPS•HP-26 structure. (A) The polypeptide chain in the structure is shown as a ribbon diagram with helices (spirals) in cyan, strands (arrows) in orange, and loops (tubes) in grey. The DHPS module of the bifunctional enzyme is shaded. The HP-26 is shown as a stick model in the atomic color scheme (C in grey, N in blue, O in red, and S in yellow) outlined with the simulated annealing omit map (blue nets: $F_o - F_c$; contoured at 2.0 σ). (B) A zoomed-in view for the inhibitor and electron density.

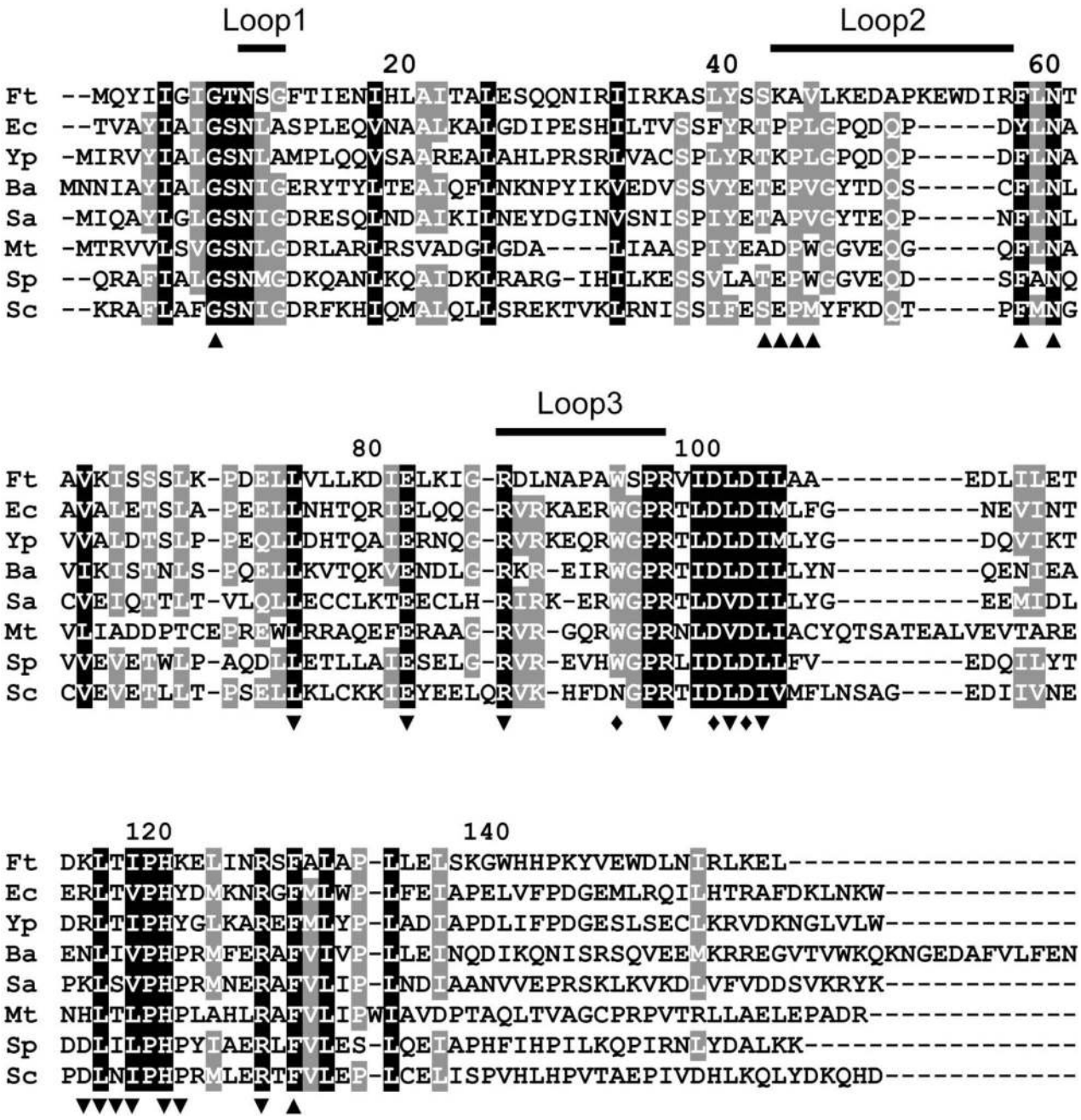

Figure 4.

Structure-based alignment of HPPK amino acid sequences. The amino acid numbering is that of FtHPPK-DHPS. The most conserved and highly conserved residues are shaded in black and gray, respectively.The active-site loops are indicated by horizontal bars. The residues involved in binding of HP and MgATP are marked below the sequence alignment with ▲ and ▼, respectively. Residues with 4.5 Å of both substrates are marked with ◆. Ft, *F. tularensis*; Ec, *E. coli*; Yp, *Y. pestis*; Ba, *B. anthracis*; Sa, *S. aureus*; Mt, *M. tuberculosis*; Sp, *S. pneumoniae;* Sc, *S. cerevisiae*.

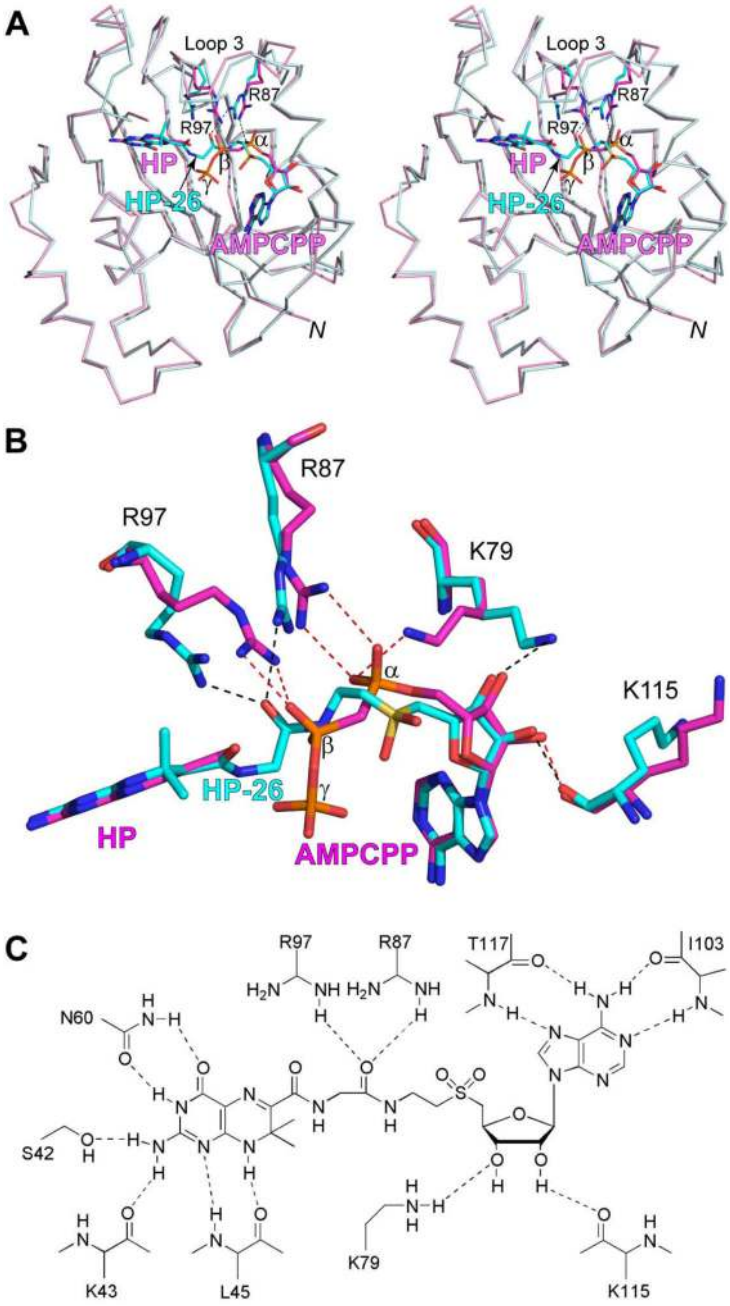

Figure 5.

Interactions between FtHPPK and HP-26. (A) Stereoview showing the superimposed FtHPPK•HP-26 (C atoms in cyan, this work) and FtHPPK•HP•MgAMPCPP (C atoms in magenta, PDB entry 3MCO) structures. (B) An enlarged view showing selected details of protein-ligand interactions in the two structures. Hydrogen bonds are indicated with dashed lines either in black (in FtHPPK•HP-26) or red (in FtHPPK•HP•MgAMPCPP). (B) Protein-inhibitor interactions as observed in the FtHPPK•HP-26 structure.

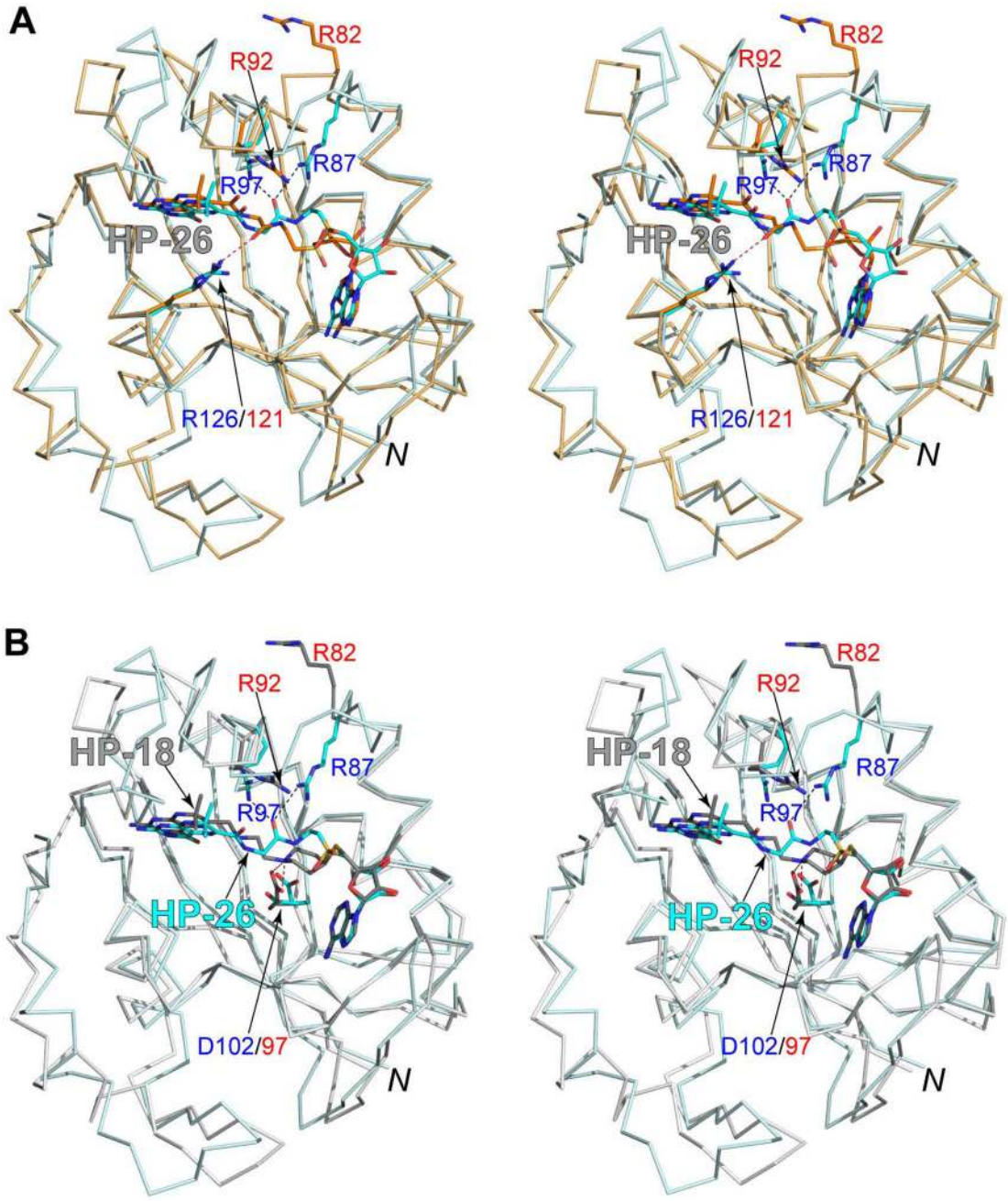

Figure 6.

Stereoviews showing structural comparisons. (A) Superimposed FtHPPK•HP-26 (C atoms in cyan, this work) and EcHPPK•HP-26 (C atoms in orange, PDB entry 4F7V). Proteins are shown as Cα traces. HP-26 and selected side chains are shown as sticks. Hydrogen bonds are indicated with dashed lines either in black (in FtHPPK•HP-26) or red (in EcHPPK•HP-26). (B) Superimposed FtHPPK•HP-26 (C atoms in cyan, this work) and EcHPPK•HP-18 (C atoms in gray, PDB entry 3UDE). Hydrogen bonds are indicated with dashed lines either in black (in FtHPPK•HP-26) or red (in EcHPPK•HP-18).

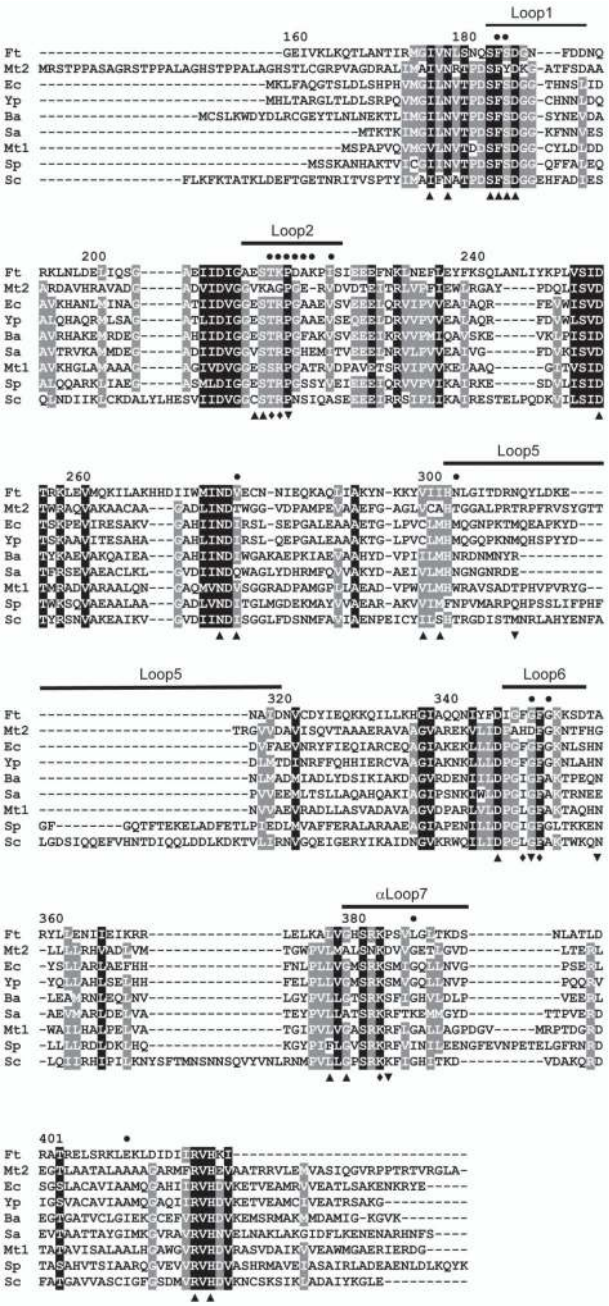

Figure 7.

Structure-based alignment of DHPS amino acid sequences. The amino acid numbering is that of FtHPPK-DHPS. The most conserved and highly conserved residues are shaded in black and gray, respectively. The active-site loops are indicated by horizontal bars. The residues involved in binding of HPPP and *p*ABA are marked below the sequence alignment with ▲ and ▼, respectively. Residues within 4.5 Å of both substrates are marked with ◆. Sites of mutations that cause resistance to sulfa drugs are indicated by ● above the sequence alignment. Ft, *F. tularensis*; Mt2, *M. tuberculosis* DHPS 2; Ec, *E. coli*; Yp, *Y. pestis*; Ba, *B. anthracis*; Sa, *S. aureus*; Mt1, *M. tuberculosis* DHPS 1; Sp, *S. pneumoniae;* Sc, *S. cerevisiae*.

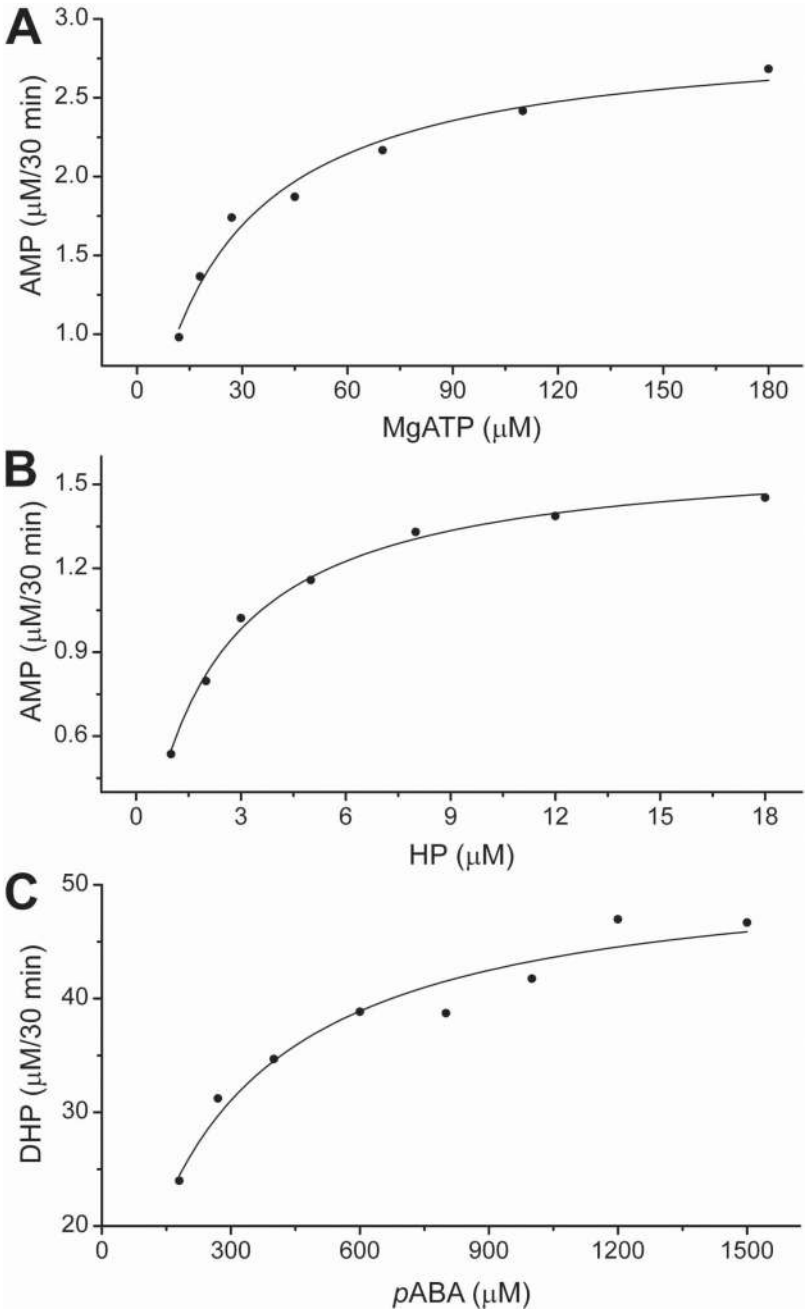

Figure 8.

Steady-state kinetic analysis of FtHPPK-DHPS. (A) HPPK kinetics with MgATP varied while HP is fixed for determining the K_m for MgATP. (B) HPPK kinetics with HP varied while MgATP is fixed for determining the K_m for HP. (C) DHPS kinetics with *p*ABA varied while HPPP is fixed.

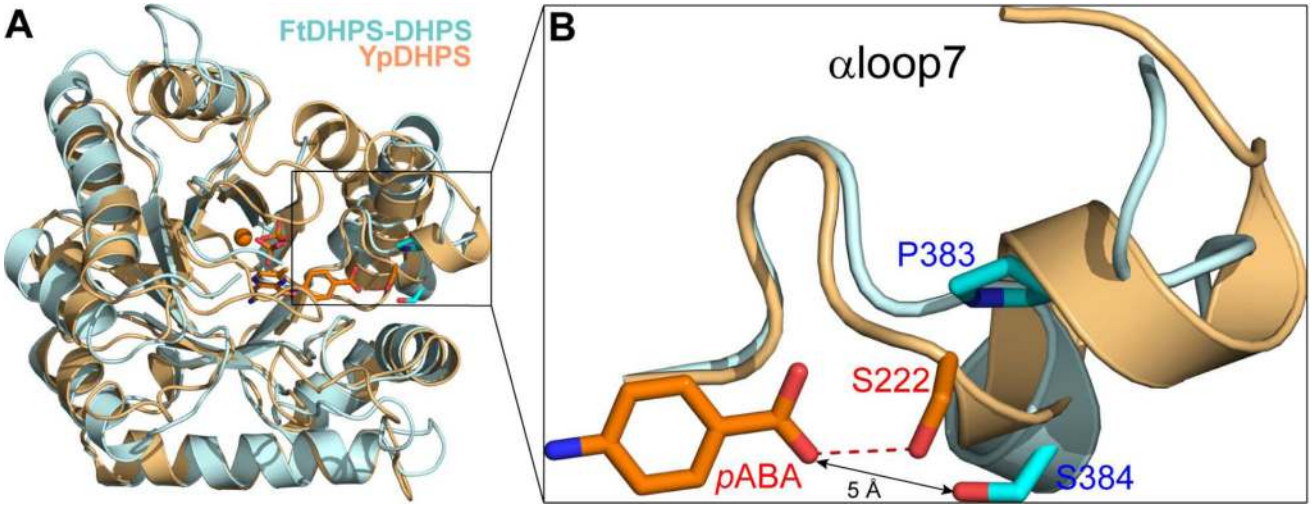

Figure 9.

Structural features in the DHPS of FtHPPK-DHPS. (A) Superimposed FtHPPK-DHPS•HP-26 (C atoms in cyan, this work) and YpDHPS•Mg^{2+}•*p*ABA•PP•XHP (C atoms in orange, PDB entry 3TYZ). Proteins are shown as ribbon diagrams. Selected ligands, including PP (pyrophosphate ion) and XHP [2–amino-6-metyhlidene-6,7-dihydropterindin-4(3H)-one], and side chains are shown as sticks. The hydrogen bond is indicated with a dashed line in red. (B) A zoomed-in view showing only the αloop7 in the two structures and the *p*ABA in YpDHPS•Mg^{2+}•*p*ABA•PP•XHP. Indicated by a double-headed arrow is the distance between the S384 hydroxyl of FtHPPK-DHPS•HP-26 and the pABA of YpDHPS•Mg^{2+}•*p*ABA•PP•XHP.

Table 1

Binding and inhibition activities of bisubstrate analogue HPPK inhibitors

Inhibitor	*E. coli* HPPK			*F. tularensis* HPPK		
	IC_{50} (μM)[a]	K_i (μM)[b]	K_d (μM)[a]	IC_{50} (μM)	K_i (μM)[b]	K_d (μM)
HP-18	3.2±0.3	1.1	2.6±0.2	180±90	85	ND[c]
HP-26	9.5±1.0	3.1	4.2±0.3	5.1±0.4	2.4	2.0±0.3

[a] From Shi and coworkers [15, 16].

[b] Calculated from IC_{50} values using the Cheng-Prusoff equation [28].

[c] Not determined.

Table 2

Crystal data, X-ray diffraction, and structure

PDB Entry Code	**4PZV**
Crystal	FtHPPK-DHPS•HP-26
Space group	$P2_1$
Unit cell parameters: *a* (Å)	42.95
b (Å)	74.44
c (Å)	69.76
Data	Overall (last shell)
Resolution (Å)	30.00-1.70 (1.76-1.70)
Unique reflections	43013 (3416)
Redundancy	3.5 (1.9)
Completeness (%)	90.0 (72.1)
R_{merge} [a]	0.087 (0.405)
I/σ	9.9 (1.9)
Refinement	Overall (last shell)
Resolution (Å)	28.11-1.70 (1.79-1.70)
Unique reflections	43002 (4895)
Completeness (%)	89.7 (72.0)
Data in the test set	979 (103)
R-work	0.213 (0.361)
R-free	0.259 (0.384)
Structure	
Protein non-H atoms / B (Å^2)	3523 / 18.0
Ligand atoms / B (Å^2)	80 / 16.6
Water oxygen atoms / B (Å^2)	434 / 23.2
RMSD	
Bond lengths (Å)	0.009
Bond angles (°)	1.075
Coordinate error (Å)	0.29
Ramachandran plot [b]	
Favored regions (%)	97.3
Disallowed regions (%)	0.0

[a] $R_{merge} = \Sigma|(I-<I>)| / \Sigma(I)$, where I is the observed intensity.

[b] Obtained using Ramachandran data by Lovell and coworkers [57].

Table 3

Kinetic constants of FtHPPK-DHPS in comparison with those of other enzymes

Enzyme	$K_{m(MgATP)}$ (μM)	$K_{m(HP)}$ (μM)	k_{cat} (S^{-1})
FtHPPK	19±3	1.8±0.2	0.17±0.01
EcHPPK	11±1	0.49±0.1	0.71±0.1
	$K_{m(pABA)}$ (μM)		
FtDHPS	200±40	NA[a]	0.0029±0.0002
EcDHPS[b]	0.5		1.9
BaDHPS[c]	1.8		0.55
MtDHPS1[d]	0.37		0.29
ScDHPS[e]	3.8		1.3

[a]Not applicable.

[b]From Talarico and coworkers [33].

[c]From Yun and coworkers [34].

[d]From Nopponpunth and coworkers [35].

[e]From Berglez and coworkers [37].